Title
Application of atomic force microscopy to studies of surface processes in virus crystallization and structural biology

Journal
Acta Crystallographica Section D, Structural Biology, 58(10-1)

ISSN
2059-7983

Authors
Malkin, AJ
Plomp, M
McPherson, A

Publication Date
2002-10-01

DOI
10.1107/s090744490201274x

Application of atomic force microscopy to studies of surface processes in virus crystallization and structural biology

A. J. Malkin*, M. Plomp and A. McPherson

University of California, Irvine, Department of Molecular Biology and Biochemistry, Irvine, CA 92697-3900, USA.
E-mail: amalkin@uci.edu

Atomic force microscopy (AFM) investigation revealed the sources of disorder and mechanisms of their formation in crystals of an icosahedral plant virus, Cucumber Mosaic Virus (CMV) and structure of the Herpes Simplex Virus (HSV-1). The combination of defects and local disorder in CMV crystals presented here are likely the physical bases for mosaicity in virus crystals, and may be largely responsible for their limited diffraction resolution. High-resolution images of intact, enveloped HSV-1 and the underlying capsid structure demonstrate capabilities of AFM to probe structures of large macromolecular assemblies.

Keywords: **AFM, viruses, defects, crystallization**

1. Introduction

High-resolution structures of viruses obtained from X-ray crystallographic analyses are necessary to provide the architectural basis for a comprehensive understanding of pathogenesis on the molecular level. In the case of viral infections, this involves detailed knowledge of the virion composition and architecture. In spite of much recent progress in physical analyses of virus crystallization (Malkin *et al.*, 1995; Malkin *et al*., 1999, Kuznetsov *et al*., 2000) it is still unclear which kinds of disorder limit the diffraction resolution of virus crystals, and what are the sources of the disorder that arise during growth.

X-ray crystallography cannot be applied to the structural studies of most complex human and animal viruses. This is because, in addition to their structural heterogeneity, they are very difficult to produce in sufficient quantities for crystallization. Moreover, their sheer size often places them outside the range of X-ray crystallography. An alternative that has proven effective, though at significantly lower resolution (typically no better than 8 Å), is cryo-electron microscopy (cryo–EM) (Baker *et al.*, 1999). However, a major limitation of this method is that it benefits greatly from high particle symmetry, such as icosahedral symmetry, and is far less powerful for non-symmetrical viruses.

Atomic force microscopy (AFM) allows not only direct visualization of mechanisms of defect formation on molecular level, but also *in vitro* probing of structures and dynamics of large human viruses. This approach, as is seen here in the crystallization of Cucumber Mosaic Virus (CMV), revealed combination of defects and local disorder (sections 3.1 – 3.5), which may be largely responsible for their limited diffraction resolution. Studies on molecular dynamics on surfaces of CMV crystals allowed measurements of the attachment frequencies and probabilities for incorporation of virions in the growth step (section 3.4). The primary features of single particles of herpes simplex virus (HSV-1) were visualized by AFM (section 3.5) with resolution comparable to EM techniques.

2. Experimental section

The study we describe here used CMV and HSV-1. CMV is T=3 virus of 28 nm diameter whose capsid is composed of 180 identical protein subunits and whose genome is a single stranded RNA (Wikoff *et al*., 1997). Preparations and purification procedures for CMV are described in greater details elsewhere (Lot *et al.*, 1972). CMV crystals having a hexagonal plate shape were grown using vapor diffusion method consisting of mixing 3-7mg/ml CMV in H_2O with 1M ammonium phosphate (pH=7.6) and had sizes in the range of 50 –75 μm (Malkin & McPherson, 2002). From X-ray diffraction analysis using synchrotron radiation the crystals are of rhombohedral space group R3 with a = b = c = 291.4 Å and $\gamma = 109°$ (equivalent hexagonal unit cell a = b = 475.4 Å, c = 299.2Å). The crystals generally diffract to no better than 10 Å resolution, and in the best of cases to about 4 Å. Seed crystals were mounted on the plastic disk and then transferred into the AFM fluid cell, which was subsequently filled with a mixture of virus and precipitant solution. All operations were carried out under crystallization conditions, in a fluid filled cell, with the supersaturation controlled by the by the virus concentration. The diffusion coefficient of CMV was determined using a Malvern 4700c submicro particle analyzer (Malvern Instruments, Inc., Southborough, MA).

The intact enveloped HSV-1 virion, containing the double stranded DNA genome, is about 200 nm in diameter. HSV-1 icosahedral capsid, of triangulation number T = 16, has a diameter of 125 nm and is composed of 12 pentameric and 150 hexameric capsomeres interconnected by 320 smaller protein complexes known as triplexes (Zhou *et al*., 1994, Booy *et al*., 1994). The frozen virus suspension was thawed and either first mixed 1:1 with 0.2% Triton X-100 detergent or directly deposited on freshly cleaved mica. After a few minutes, samples were gently rinsed with double distilled water and quickly dried with a flow of nitrogen gas. (Plomp *et al*., 2002) Imaging was performed using a Nanoscope IIIa AFM (Digital Instruments, Santa Barbara, CA) operated in tapping mode. Commercially available Si tips and oxide sharpened silicon nitride tips were utilized respectively for imaging of HSV-1 in the air and CMV crystals in the fluid.

3. Results and discussion

3.1. Domain structure of CMV crystals and mechanisms of its formation

AFM images of the (001) face of CMV crystals revealed numerous domains with sizes in the range of 0.2 μm^2 to 50 μm^2 (Fig.1). In some cases the virion lattice within an individual domain is misoriented with respect to the virion lattice outside the domain, as shown in Figure 1b. The height difference between domains within the same surface growth layer varies from 0.6 nm to almost 5 nm, which is equivalent to 2% to 18% of the diameter of the virus particles making up the lattice.

Layer growth on the (001) face of hexagonal crystals of CMV occurs by the progression of steps generated exclusively by 2D nucleation (Fig. 2). Heights on the (001) face are not equal for different steps, but vary in the range of 25 nm – 30 nm. Virions forming a new growth layer, corresponding to the smallest measured step heights of 25 nm, position themselves in triangular depressions formed by virions in the layer below (position A in Fig. 2c). Steps having heights of 30 nm, on the other hand, have their constituent virions positioned atop particles in the preceding layer (position B in Fig. 2c). The broad and continuous range of height differences among growth steps (0.5 –5nm) suggests that virions creating a new 2D nucleus may attach, presumably due to weak and geometrically

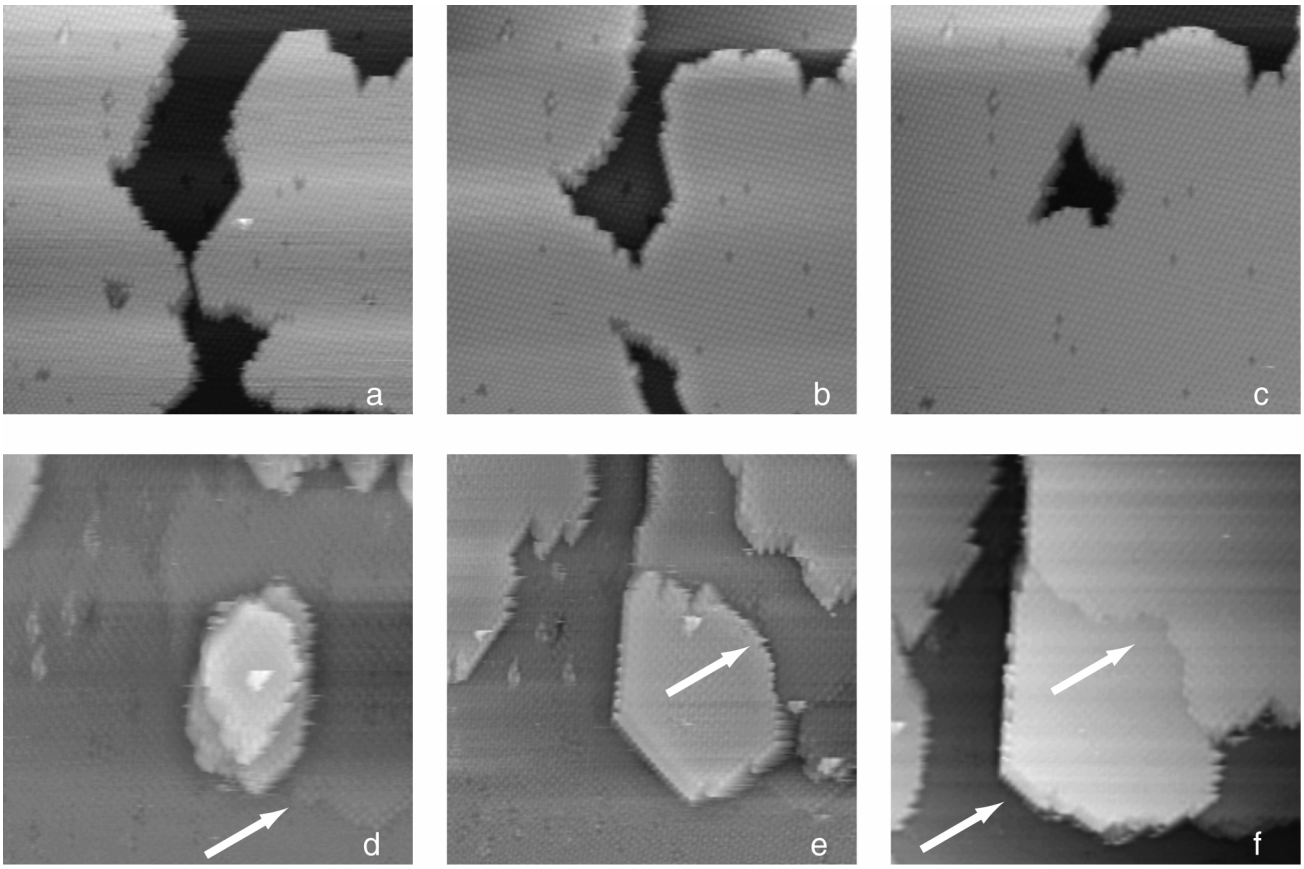

Figure 1
AFM images of the (001) face of CMV crystals. (a) large area revealing multiple domains (indicated with arrows). In (b)–(c) higher magnification AFM images of domains (indicated with arrows). The scan areas are 18 x 18 μm (a), 1.3 x 1.3 μm (b), and 1.5 x 1.5 μm (c).

imprecise bonds, arbitrarily at intermediate sites between positions A and B (Fig. 2c) on the proceeding layer. Remarkably, even within a single domain a height difference between virions of up to 1.5 nm is observed. A 2D nucleus, therefore, can grow by addition of virions,

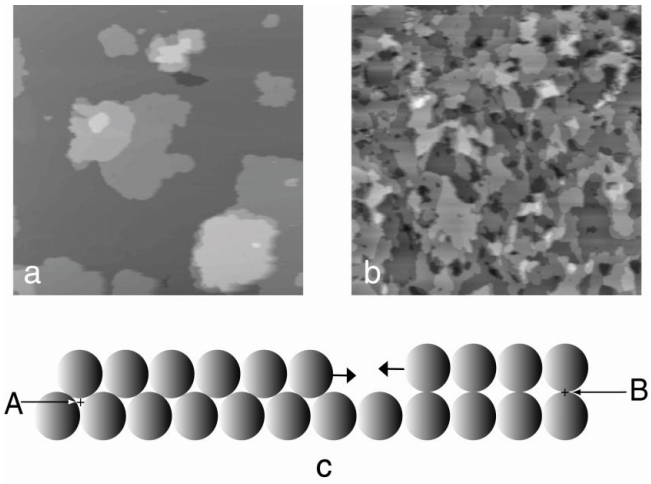

Figure 2
AFM images of the (001) face of CMV crystals showing 2D nucleation at relatively low (a) and high supersaturations (b). A cross section of the (001) face showing arbitrary attachment of virions on the underlying growth layer is in (c). The scan areas are 16 x 16 μm (a), and 18 x 18 μm (b).

which come to occupy significantly different crystallographic positions within the same growth layer.

Due to height variations**,** a significant number of individual 2D nuclei are formed on the (001) face, which are crystallographically misoriented with respect to one another. Because of the non-rigorous nature of the molecular contacts in the lattice, coupled with an unusually high elasticity, growth layers with height differences of up to 2 nm may, nonetheless, merge without formation of defects. Examples are shown in Figs. 3a-c. Coalescence of growth steps with larger height differences, in the neighborhood of 3 nm and larger results in formation of domain boundaries.as seen in Figs. 3 d-f. As illustrated in Fig. 3d growth layers do not advance beyond the original domain boundary, which serves as a barrier. Thus, such defects propagate throughout the volume of the crystal.

Growth by formation of misoriented 2D nuclei by growth steps with variable heights resulting in this kind of domain structure has not been previously reported, to our knowledge, either in the growth of inorganic or macromolecular crystals. The source of mosaicity in CMV crystals is the formation of growth steps of variable sizes due to the attachment of virions to arbitrary sites on the preceding layer during multiple two dimensional nucleation under supersaturated conditions (Fig. 2).

3.2. Defect formation due to the incorporation of aberrant virions.

High-resolution AFM images of the surface layers of CMV crystals reveal the unexpected presence of abnormal virions with diameters in the range of 22-36 nm, as exemplified by those seen in Figs. 4 a-b. Incorporation of abnormal virions causes local distortion, which

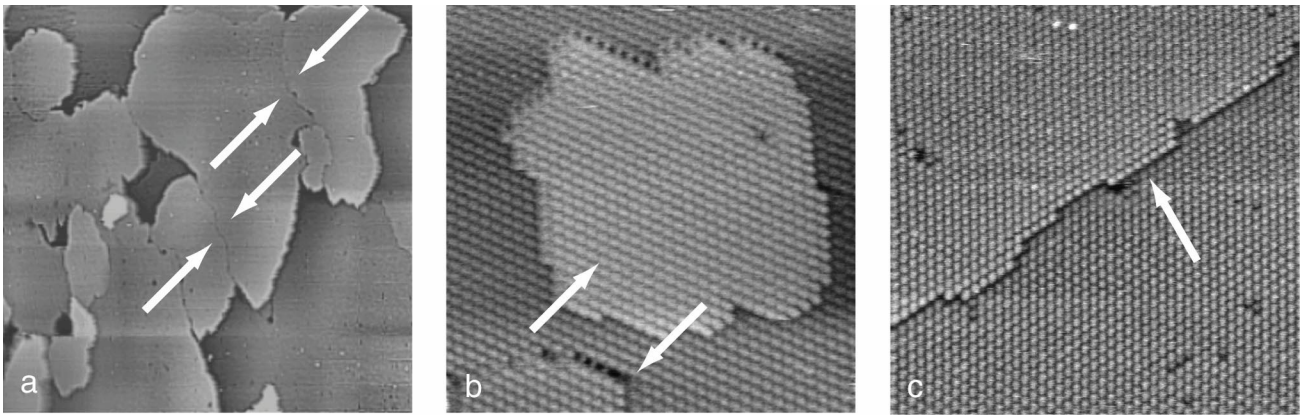

Figure 3
AFM images (a-c) showing the merger of growth steps without formation of defects. In (d) through (f) formation of domain boundaries arising from the merger of misoriented two-dimensional nuclei is seen. Pre-existing and newly formed domain boundaries are indicated with arrows in (d-f). AFM images are 2 by 2 μm in (a-c), and 2.75 by 2.75 μm in (d), 3.25 x 3.25 μm in (e) and 3 x 3 μm in (f).

propagates through several adjacent rows of virions and results in defect formation (Fig. 4a) or causes misplacements of the virion in the immediate vicinity of incorporated abnormal particles (Fig.4b). Density of these defects can be very high, up to 10^9 cm^{-2}, which is a several orders of magnitude greater than point defect densities visualized for other macromolecular crystals (Malkin *et al.*, 1996). AFM also proved effective in the molecular scale manipulation of defects in CMV crystals. For example, in 3 minutes between the AFM scans shown in Figs. 4b and 4c, an anomalously large virion (indicated by the number 3 in Fig. 4b) was displaced from the surface layer by applying an increased force with the AFM tip. This resulted in an immediate local rearrangement of virions in the crystalline lattice and disappearance of the point defect. This was accompanied by a further repositioning of two other virions (indicated with arrows).

In addition to the virions, which upon adsorption on the crystalline surface develop into 2D nuclei, we also consistently observed virus particles having diameters of 28 nm, and their clusters, which adsorbed to the crystalline surface, but never developed into 2D nuclei (Malkin & McPherson, 2002). Ultimately these virions, and their clusters were incorporated into growth steps, often causing defect formation. Microheterogeneity of virions could arise from capsid modifications during purification procedures and storage.

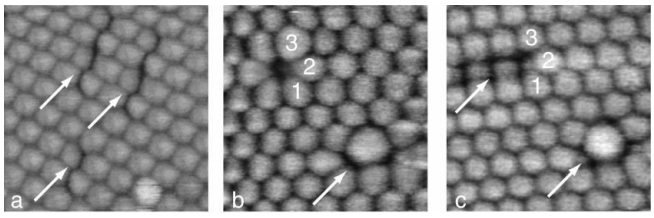

Figure 4
AFM images showing incorporation of aberrant virions. (a) the incorporation of abnormal CMV virions with diameters in the range of 22-26 nm (indicated with arrows) results in defect formation. In (b) the incorporation of two abnormally large virions into the crystalline lattice is seen. These two virions have the diameter of approximately 36 nm In (c), the abnormally large virion indicated by the number 3 in (b), was displaced from the surface layer by the AFM tip. This was followed by a rearrangement of the surrounding virions in the crystalline lattice. AFM images are 230 x 230 nm (a), 190 x 190 nm (b), and 210 x 210 nm (c).

3.3. Correlation between observed macro- and micro heterogeneities in CMV crystals and their poor diffraction properties.

In CMV crystals, mosaic blocks disrupted both long- and short-range lattice order, and the mechanisms by which they formed were evident. Mosaic block structure generally assumes that variation in domain orientation occurs on a length scale comparable to the crystal size. It arises from the domain structure of the crystalline faces, and those domains are, in turn, due to the coalescence of misoriented 2D islands. Thus the observations presented here are important in identifying the sources of mosaicity, which, to a great extent, determines the resolution limit and the ultimate quality of X-ray structure determinations. Because of the arbitrary disposition of virions within individual domains and growth layers, their deviations from average lattice orientations and positions are considerable. This produces local disorder within the CMV crystals. Particle variability within the CMV lattice due to virion microheterogeneity results in a lattice strain and poorer long-range order. The local disorder we observe for CMV crystals is likely common in crystals of most T=3 viruses and this could explain their generally poor diffraction properties (Canady *et al*., 1996, Lucas *et al*., 2002, Larson *et al*., 1998). It is quite likely that the disorder of most T=3 icosahedral virus crystals, which typically diffract to no better than 3.0 Å resolution, reflect the fundamental sources identified in this investigation, but generally to lesser degrees.

3.4. Incorporation of CMV virions into CMV crystals: attachment frequencies and probabilities.

In macromolecular crystallization, macromolecules in an arbitrary orientation cannot join a growth site. While the necessity of desolvation is likely less important than in the crystallization of inorganic molecules (Chernov, 1984), the entropic activation barrier must play an important role. Pre-kink selection would be expected for the approaching macromolecule to assume an acceptable orientation for incorporation into the growth step. In CMV crystals, icosahedral virions are connected in the surface layer through hexameric capsomeres (Smith *et al*., 2000) hence there are 60 identical orientations for correct incorporation, far more than for most proteins. This, given the weak and imprecise nature of bonding between virions in the (001) plane, should result in relatively high attachment probabilities.

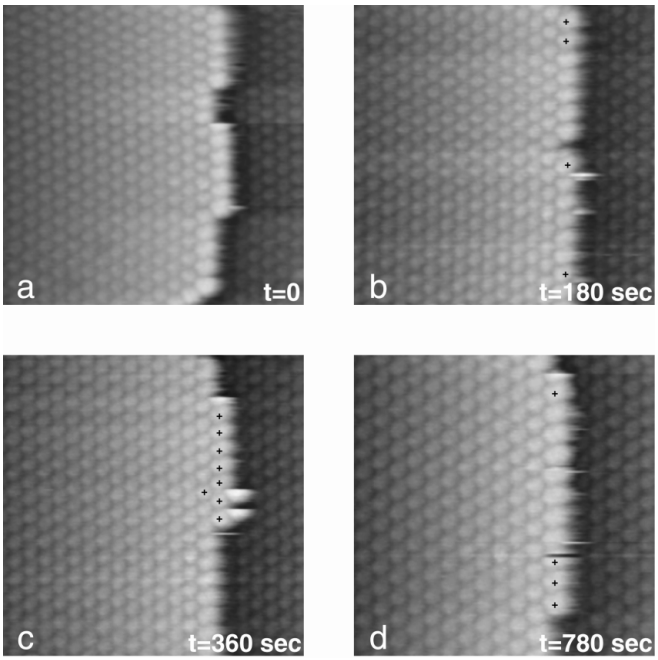

Figure 5
AFM images of an advancing growth step on the (001) face of a CMV crystal. Newly incorporated virions are indicated by +. The scan areas are are 670 x 670 nm (a-c), and 560 x 560 nm (d).

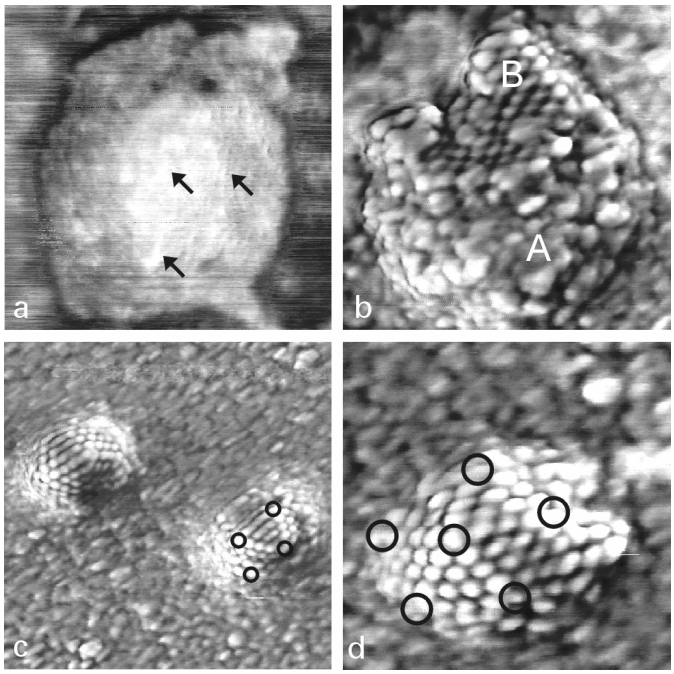

Figure 6
HSV-1 virions in different conformations adsorbed on mica and imaged with tapping-mode AFM in air. In (a) the capsid is still covered by the lipid envelope. Elongated features of 10 –25 nm sizes may correspond to glycoproteins and are denoted by arrows. In (b) –(c) addition of 0.2% Triton X-100 removes the lipid envelope. (b) Most of this capsid is covered by an irregular collection of particles of approximately 10 nm size (area A), which correspond to tegument proteins. In a smaller region the underlying, highly regular capsid is exposed (area B). In (c) a completely stripped capsid with black circles denoting the pentons. AFM images are 350 x 350 nm (a, b); 600 x 600 nm (c) and 270 x 270 nm (d).

As seen in Fig. 5, advancement of growth steps proceeds by one-dimensional nucleation of kinks (Voronkov, 1970, Kuznetsov *et al*., 1999, Chernov *et al*., 1999) formed by single or multiple virions, with subsequent lateral extension of molecular rows by addition of virions into kinks. Under the supersaturation conditions here (~ 0.1 mg/ml CMV), the attachment frequency of virus particles was found to be ~2.3 x 10^{-2} virions/sec. There was no detachment of any virus particle, either at supersaturated or equilibrium conditions, hence, thermal energy is insufficient to displace a particle from the step edge.

In these experiments the concentration of virions in solution was c = 7 x 10^{12} cm^{-3}, corresponding to an average distance between virions of L = 5 x 10^{-5}cm. Assuming that growth proceeds by direct incorporation of virions from the bulk solution into the step edge (Chernov, 1984), and that the concentration of virions at the crystalline interface is zero, then the diffusive flux can be estimated as J = D $(C\text{-}C_0)/L$ = 2.2x10^{10} $s^{-1}cm^{-2}$. D = 1.6x$10^{-7}$$cm^2/s$ is the diffusivity of CMV determined from light scattering experiments. From this, virus particles encounter a kink, having a size of approximately 30 x 30 nm, with a frequency of approximately ~ 0.2 s^{-1}. Using the attachment frequencies of 2.3 x 10^{-2} s^{-1} measured from AFM (Fig. 6), the attachment probability is ~ 10^{-2}. Thus, approximately one out of every 100 CMV virions that approach the step edge incorporates into the step.

This probability of attachment can be related in large part to pre-kink selection of proper molecular orientation for incorporation into the growth step. For high symmetry particles, as might be expected, pre-kink selection of the proper molecular orientation is considerably less than for most macromolecules. Indeed, from the same calculation using AFM data for step advancement in thaumatin crystallization (Kuznetsov *et al*., 1999) the attachment probability of those protein molecules, which can have only one correct molecular orientation for incorporation into the crystal, was estimated to be ~ 5x10^{-4}.

3.5. Structural studies of HSV-1.

The clarity with which structural detail were visualized on the surfaces of small T=3 plant viruses (Malkin *et al*., 1999) suggests that AFM may be even more broadly useful as an analytical tool for macromolecular structural investigations of large animal and human viruses. While most of these viruses cannot be crystallized, AFM can provide a means for directly obtaining structural information on individual virus particles immobilized on a substrate. Here we tested the capabilities of AFM on one of the most widespread human viruses, Herpes Simplex Virus 1 (HSV-1). The 8.5 Å cryo – EM model of the HSV-1 capsid structure (Zhou *et al*., 2000) provides a standard against which the AFM studies described here can be compared.

In Fig. 6a, an AFM image of the enveloped HSV-1 virions is presented. A number of features having length in the range of 10-25 nm are visible on the surface of the lipid envelope. These features correlate well with the dimensions of virus-encoded glycoproteins, which are essential for virion infectivity and penetration into the host cell and are incorporated into the virion envelope. As illustrated in Fig. 6b removal of the lipid envelope upon treatment with detergent allows the visualization of both the tegument and capsomere structure (seen on the upper part of the virus capsid). Here a capsid is seen to be covered with an irregular coating of particles of various sizes up to 10 nm. These are more likely tegument proteins, which are known to have a complex non-icosahedrally ordered arrangement. There are at least 18 different viral proteins, the largest of which, VP 1-3, has an predicted size of 336 kD (Zhou *et al*., 1999). This corresponds well to the observed particles of ~10 nm

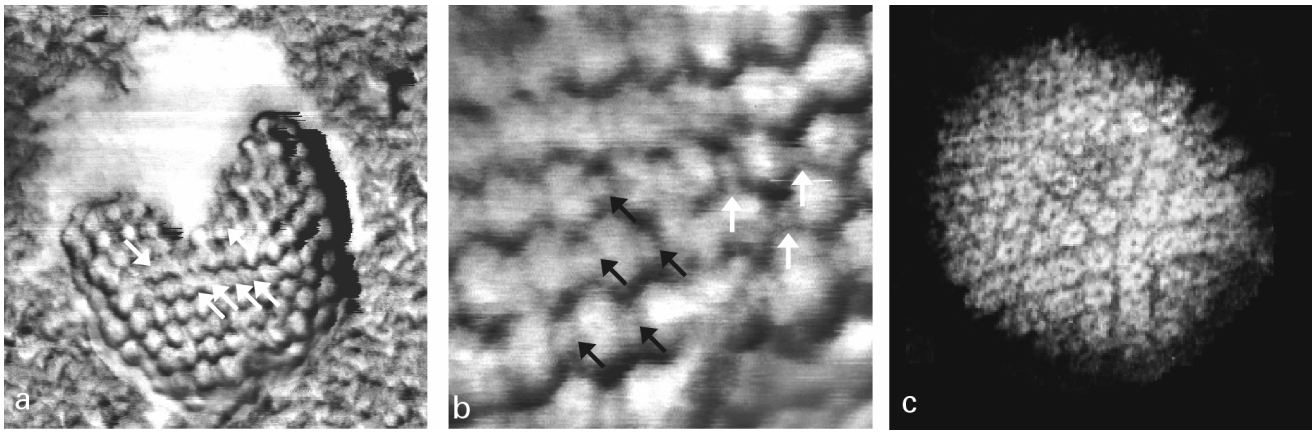

Figure 7
In (a) a HSV-1 capsid is partly covered by the lipid envelope. Hollow channels in the centers of capsomeres are indicated with arrows. In (b) triplexes, indicated with arrows are consistent with image reconstruction EM models of HSV-1 (Zhou et al., 2000). (c) the HSV-1 capsid structure visualized by electron microscopy. AFM images are 335 x 335 nm (a) and 100 x 100 nm (b).

and smaller. Because of inherent softness, the membrane may be deformed slightly by AFM tip pressure, making the visualization of glycoproteins (Fig. 6a) more difficult compared with the tegument proteins.

The structure of icosahedral capsid, revealed upon vigorous treatment of virions with detergent, is presented in Figs. 6c and 7 at different magnifications. The main components of the icosahedral capsid of triangulation number T = 16, as determined by cryo-EM, are 12 pentameric capsomeres and 150 hexameric capsomeres. These capsomeres are interconnected by 320 smaller protein complexes known as triplexes (Zhou *et al*., 2000). As illustrated in Fig. 7, the pentameric and hexameric capsomeres can be discriminated from one another in AFM images. Diameters of capsomeres of approximately 15 nm are accurately reflected by AFM. In Figs. 7a, and b substructure of individual capsomeres (holes in the middle consistent of the structure of the capsid determined from EM) can be seen. In addition small protein clusters, which correspond to triplexes that link adjacent capsomeres are visualized. The capsids seen in the AFM images do not exhibit the level of perfection implied by the cryo – EM structure, though all are consistent with that model in a general sense. Not only does AFM allow us to visualize the a-periodic features of the virions, it shows us the natural variation about the mean structure. When compared to EM single images (Fig. 7c), the resolution is similar. In addition AFM can also probe the dynamic processes involving the large viruses assemblies. Thus, for example, we were able to observe the disassembly of viruses and the extrusion of HSV-1 DNA (Plomp *et al*., 2002). This information is of considerable interest for understanding the processes in the cytoplasm at the time of infection as well as the DNA packing in the virion. Note, that *in situ* AFM can be successfully applied also to studies of large non-symmetrical viruses, such as vaccinia virus (Malkin *et al*., 2002).

Currently, the limitation of application of the powerful technique of AFM in structural biology and molecular pathology is the resolution limit imposed by the finite tip radius, which is typically larger than 10-15 nm. Based on recent improvements in the fabrication of ultrasharp nanotube tips (Hafner *et al*., 1999, Woolley *et al*., 2000), it is reasonable to expect that AFM resolution will considerably improve in the very near future, making AFM resolution superior to that of conventional EM. This high-resolution capacity, combined with its capability of *in vivo* imaging make AFM well suited for use in the fields of structural virology and molecular pathogenesis.

Acknowledgements

We wish to thank A. Greenwood and J. Zhou for technical assistance and S. B. Larson, Yu. G. Kuznetsov and P. Vekilov for discussions. The National Aeronautics and Space Administration (Grant NAG8-1569) supported this research.

References

Baker, T. S., Olson N. H. & Fuller, S. D. (1999). *Microbol. Mol. Biol. Rev.* **63**, 862-922.
Booy, F. P., Trus, B. L., Newcomb, W.W., Brown, J. C., Conway, J. F. & Steven, A. C. (1994). *Proc. Natl Acad. Sci. USA*, **91**, 5652-5656.
Canady, M. A., Larson, S. B., Day, J. & McPherson, A. (1996). *Nature Struct. Biol.*, **3**, 771-781.
Chernov, A. A. (1984). *Modern Crystallography III: Crystal Growth*, Springer-Verlag: Berlin.
Chernov, A. A., Rashkovich, L. N., Yaminski, I. V. & Gvozdev, N. V. (1999). *J. Phys. Condensed Matter*, **11**, 9969-9984.
Hafner, J. H., Cheung, C. L. &, Lieber, C. M. (1999). *Nature*, **398**, 761-762.
Kuznetsov, Yu. G., Konnert, J., Malkin, A. J. & McPherson, A. (1999). *Surf. Sci*. **440**, 69-80.
Kuznetsov, Yu. G., Malkin, A. J., Lucas, R. W. & McPherson, A. (2000). *Colloids and Surfaces B: Biointerfaces*, **19**, 333-346.
Larson, S. B., Day, J., Greenwood, A. & McPherson, A. (1998). *J. Mol. Biol.*, **277**, 37-59.
Larson, S. B., Day, J., Canady, M. A., Greenwood, A. & McPherson, A. (2000). *J. Mol. Biol.* **301**, 625-642.
Lot, H., Marrow, J., Quiot, J. B. & Esvan, C. (1972). *Ann. Phytopathol*. **4**, 25-38.
Lucas, R. W, Larson, S. B. & McPherson, A. (2002)**.** *J. Mol. Biol.* **317**, 95-108.
Malkin, A. J., Land, T. A., Kuznetsov, Yu. G., McPherson, A. & DeYoreo, J. (1995). *J. Phys. Rev. Lett.* **75**, 2778-2781.
Malkin, A. J., Kuznetsov, Yu. G. & McPherson, A. (1996). *J. Struct. Biol.* **117**, 124-137.
Malkin, A. J., Kuznetsov, Yu. G., Lucas, R. W. & McPherson, A. (1999). *J. Struct. Biol.* **127,** 35-43.
Malkin, A.J. & McPherson, A. (2002). *J. Phys. Chem.* In the press.
Malkin, A.J., McPherson, A. & Gershon, P.D. (2002). In preparation.
McPherson, A., Malkin, A. J. & Kuznetsov, Yu. G. (2000). *Annu. Rev. Biophys. Biomol. Struct*. **29**, 361-410.
Plomp, M., Rice, M. K., Wagner, E. K., McPherson, A. & Malkin, A. J. (2002). *Am. J. Pathol*. **160**, 1959-1966.
Smith, T. J., Chase, E., Schmidt, T., & Perry, K. L. (2000). *J. Virol.* **74**, 7578-7586.
Voronkov, V. V. (1970). *Sov. Phys. Cryst*. **15**, 13-19.
Wikoff, W. R., Tsai, C. J., Wang, G., Baker, T. S. & Johnson, J. E. (1997). *Virology*, **232**, 91-97.